Demonstration of bare Laser-reduced Graphene Oxide sensors for Ammonia and Ethanol

Almudena Rivadeneyra, Denice Gerardo, Francisco J. Romero, Víctor Toral, Sahira Vásquez, Martina Costa-Angeli, Carmen L. Moraila-Martínez, Diego P. Morales, Noel Rodríguez

***Abstract*— In this work, gas sensors using laser-reduced graphene oxide (LrGO) as sensitive layer have been fabricated and studied. The laser-synthetized material were structurally and electrically characterized by means of Scanning Electron Microscopy (SEM), Raman spectroscopy, X-ray Photoelectron Spectroscopy (XPS) and the four-point contact method. The gas-sensing properties of the samples were studied by their exposition to 10 ppm to 100 ppm of ethanol and 25 ppm to 130 ppm of ammonia. The results show that the devices present an electrical response corresponding to a purely resistive behavior up to 100 kHz. It is also demonstrated that the resistivity of the sensing layer increases as the gas concentration increases; being of 0.0402 ± 0.001 [%/ppm] for the case of ammonia and 0.0140 ± 0.001 [%/ppm] for the case of ethanol. These results outperform existing sensors and establish a better balance in terms of simplicity, sensitivity, linearity and technology sustainability. In summary, this work especially shows the potential of LrGO for low-cost and low-energy gas sensors fabrication.**

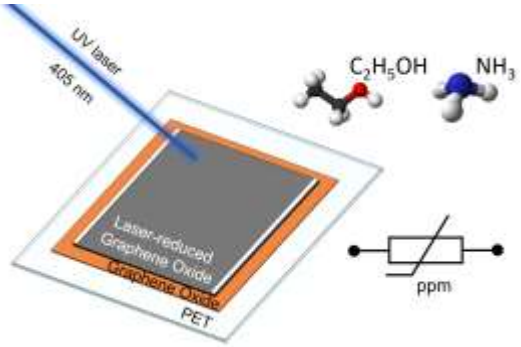

***Index Terms*— C_2H_5OH gas sensor, graphene, NH_3 gas sensor, reduced graphene oxide (rGO)**

I. Introduction

The environmental pollution caused by toxic, flammable, volatile organic compounds (VOCs) have gained wide attention in the scientific research community due to their adverse effects in human health. According to the occupational safety and health administration (OSHA) report, the maximum exposure threshold limit is 25 ppm for ammonia and 1000 ppm for ethanol [1]. Among various hazardous gases and VOCs, ammonia (NH_3) and ethanol (C_2H_5OH) are relevant gases in both industrial and environmental monitoring [2]. Ammonia is one of the most commonly produced industrial chemicals: it is used in industry and commercial products, but also exists naturally in humans and in the environment. It is essential for many biological processes and serves as a precursor for amino acid and nucleotide synthesis. Ammonia is also produced naturally from decomposition of organic matter, including plants, animals, and animal wastes. The overexposure to this gas may cause different diseases, such as irritation of the eyes, difficulty in breathing, headache, sickness, or even the death [3]. On the other hand, ethanol is also an important industrial chemical, being commonly used as a solvent or for the synthesis of organic chemicals and gasohol [4]. It can be easily mixed with water and many other organic solvents. As in the case of ammonia, the overexposure to this gas might lead to central nervous system disorders, like nausea, cough, allergies, acidosis, pneumonitis or even cancer [5]–[7].

Currently, there are two main common techniques for the detection of this kind of volatile organic compounds: photo ionization detection (PID) and flame ionization detection (FID). However, the application of these methods in industry is limited due to their relatively high-cost and complicated maintenance. Because of that, functional nanomaterials-based gas sensor technologies are called to play an important role in this field thanks to their small size, low-cost, and simple fabrication [8]. In this direction, researchers are considering new materials and nanomaterials, like MoS_2 or graphene and its derivatives (in general materials with a high specific surface area), in order to explore more suitable transduction properties for this purpose [9]–[11]. Various studies demonstrate that graphene-based nanomaterials exhibit high-performance for developing sensors that stand out because of their remarkable electrical and thermal conductivity (which may vary from 10^3 to $600 \cdot 10^3$ S/m, and from 0.01 to 2000 W/(m·K), respectively, depending on the carbon-based precursor, the synthesis method and the resulting allotrope), larger surface-area to volume ratio, high chemical stability and excellent gas absorptivity [12]–[19]. In addition, their performance can be increased by chemical reactivity, the

This work was mainly supported by TED2021-129949A-I00 funded by MCIN/AEI/10.13039/501100011033. It was also partially funded by the Andalusian regional projects supported through the Junta de Andalucía - Consejería de Universidad, Investigación e Innovación and FEDER funds: ProyExcel_00268, B-RNM-680-UGR20, P20_00265, P20_00633, as well as by the Spanish Ministry of Sciences and Innovation through the National Project PID2020-117344RB-I00, the Ramón y Cajal fellow RYC2019-027457-I and the María Zambrano fellow C21.I4.P1.

A, Rivadeneyra, Denice Gerado, F.J. Romero, V. Toral, C.L. Moraila-Martínez, D.P. Morales and N. Rodriguez are with the Department of Electronics and Computer Technology, University of Granada, 18071 Granada, Spain. e-mail: arivadeneyra@ugr.es; denicegi@ugr.es; franromero@ugr.es; vtoral@ugr.es; cmoraila@ugr.es; diegopm@ugr.es; noel@ugr.es).

S. Vásquez and M. Costa-Angeli are with the Faculty of Science and Technology, Free University of Bozen-Bolzano, 39100 Bozen-Bolzano, Italy (e-mail: Svasquez@unibz.it; martinaaurora.costangeli@unibz.it).

functionalization of their surface properties as well as the anchor activation of the metal sites [20]–[23].

In the case of ethanol and ammonia sensing, different zeolites have been extensively used due to their large surface, volume ratio and the interlinked connection with reactant pathways of their porous nanostructures [24]. Similarly, MoS_2 based sensors have also attracted a high interest in this context as a consequence of the impact of their high carrier mobility on the electrical transduction properties when they are exposed to certain gases [25]–[27]. However, these materials suffer from instability [28], [29], require a complex setup for their preparation [30] or, in contrast to some carbon-based nanomaterials (like carbon nanotubes or graphene), cannot operate at room temperature [31]. Among the carbon-based nanomaterials, reduced Graphene Oxide (rGO) features many outstanding properties that lead to a good sensing performance, such as the large content of functional groups attached to its edges and basal planes acting as adsorption sites for the gases [32], [33]. rGO is a derivative of graphene which can be synthesized chemically or by photothermal processes in a cost-effective manner [34], [35]. In fact, it has already been demonstrated that chemically reduced graphene oxide exhibits an excellent response to NH_3, offering a high sensitivity for concentrations at parts-per-million (ppm) levels [36]. In the same way, the response of rGO-based devices for gas sensing applications, such as ethanol and ammonia, have also been studied in other works [20], [37]–[39]. For instance, Li *et al.* worked on Zn_2SnO_4 nanoparticles/reduced graphene oxide (ZTO/rGO) nanocomposites with different contents of rGO, demonstrating that that the as-prepared ZTO/rGO showed an enhanced sensing performance to ethanol in comparison with pure ZTO [20]. Sangeetha and Madhan also combined molybdenum disulfide (MoS_2) with graphene to fabricate sensors and study their response to multiple gases, like ethanol, methanol, acetone, CO, NO_2 and formaldehyde [40]. Moreover, Tian *et al.* developed layer-by-layer nanocomposites consisting of Co_3O_4 and rGO nanosheets by a simple hydrothermal process with an annealing step to be used as ethanol sensor [41], while Wang *et al.* used MoO_3 nanoflakes instead for the same purpose [42].

However, the study of raw rGO obtained by means of laser photothermal processes, without any other combination of chemicals or treatment, has not been yet studied as sensing layer for this kind of gases. Thus, in this work we propose a simple and inexpensive fabrication process for the mass-production of gas sensors, simplifying not only the fabrication of the sensors, but also their integration in a final system.

This manuscript is structured as follows: after this introduction, Section 2 presents the materials and methods employed for the fabrication and characterization of the devices. Section 3 describes their structural characterization and their response to the different testing gases. After that, the discussion of the results obtained as well as their comparison with respect to other similar sensor reported in the literature is included in Section 4. Finally, the main conclusions are drawn in Section 5.

II. Materials and Methods

A. Device fabrication

Graphene oxide with a concentration of 4 mg/mL prepared following the Hummers and Offerman method was acquired from Graphenea (San Sebastian, Spain) and then used as a raw material for the manufacture of the ammonia and ethanol gas sensors [43]. We use an orbital vortex mixer (Seoulin Bioscience, South Korea) to expand and homogenize the GO colloid obtained on top of a Polyethylene Terephthalate (PET) film with 160 µm thickness (ColorGATE Digital Output Solutions GmbH, Hannover, Germany) at a concentration of 2 mL/cm^2. Then, once the remaining water evaporates at room temperature, the GO was reduced with the aid of a laser-assisted photothermal process using a CNC-driven continuous laser 405 nm diode (from Q-BAIHETM, model 405ML-300-2290, Shenzhen, China) [44]. We fabricated samples at different reduction levels by adjusting the output laser power, ranging from 50 mW to 100 mW. Figure 1 shows a schematic view of the sensors developed (sensing layer 1 cm^2) with two printed electrical electrodes on both sides using a silver-based conductive ink (from Henkel, Germany) in order to provide a good and reliable electrical contact with the characterization equipment.

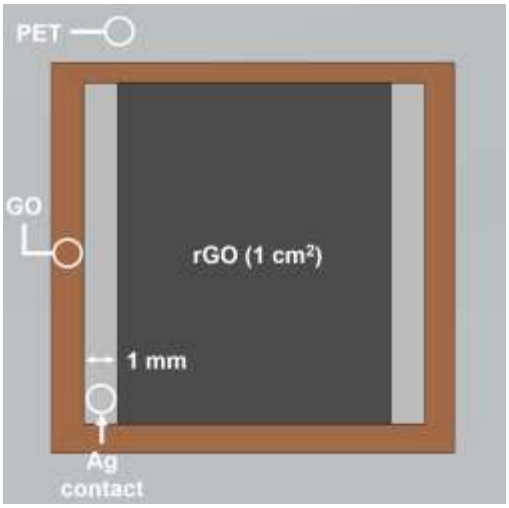

Fig. 1. Schematic of the fabricated devices.

B. rGO characterization

Scanning electron microscope (SEM) images were acquired using the field emission scanning electron microscope (SEM) NVision 40 (from Carl Zeiss, Oberkochen, Germany) at an extraction and acceleration voltage of 5 kV. Raman spectra were obtained with a dispersive micro-Raman spectrometer NRS-5100 (from JASCO International Co. Ltd., Tokyo, Japan) using an excitation source with a wavelength of λ = 532 nm (Elforlight G4-30; Nd: YAG). Measurements of X-ray Photoelectron Spectroscopy (XPS) were performed at a base pressure of 10^{-10} Torr with an Al Kα (hν = 1486.6 eV) excitation at an operating power of 450 W using an Axis Ultra-DLD spectrometer (from Kratos Analytical Ltd., Manchester, UK).

The sheet resistance measurements were performed with a four-point probe head from Jandel connected to a source measuring unit (Keysight B2901A) applying a constant current of 1 mA.

C. Device characterization

The gas sensing performance of the sensors was characterized as a function of different concentrations for both testing gases (ammonia and ethanol). For that, we used a custom-made gas chamber into which the different test gases are fluxed. The sensors were placed on top of a glass holder with a Peltier heating element and a Pt100 sensor for in-situ temperature monitoring, as described in our previous work [45]. The different concentrations (ppm) are achieved by adjusting the flux of both gases (carrier gas: N_2, and testing gas: ammonia or ethanol) but always maintaining an input gas flow of 200 mL/min during a time interval of 100 seconds.

With that, we were able to achieve a concentration of ammonia (NH_3) ranging between 10 ppm and 80 ppm, and between 25 ppm and 130 ppm for ethanol (C_2H_5OH). The sensors were exposed to a recovery interval after the exposure cycle. Such recovery consisted of 300 s in which the sensor was heated up to 80 ºC to remove the trapped gas molecules, followed by a high flux (1000 mL/min) of the carrier gas for 300 s at ambient conditions to facilitate the removal of any residual test gas molecules from the chamber [45], [46]. Before a new exposure cycle, the temperature was set again to 25 ºC. The impedance of the devices was measured as a function of the different gas concentrations using the impedance analyzer 4294A and the impedance probe kit 42941A (from Keysight Technologies, USA). The measurements were performed using a sinusoidal excitation signal of 0.5 V of amplitude at low frequency (20 Hz) to extract the resistive behavior.

In particular, the sensor performance was analyzed through its normalized resistance (N.R.), defined as the relative variation in resistance between the two contact electrodes, as described in Equation 1 (where R_0 and R_f are the initial and final values of resistance for an exposure cycle, respectively).

$$N.R. = \frac{R_f - R_0}{R_0} \qquad (1)$$

III. Experimental Results

A. Structural characterization

The images acquired by SEM for the bare GO as well as for its different reduced states at the different laser power are shown in Figure 2. Before the laser reduction, the GO over the PET substrate constitutes a homogenous and uniform coating (Figure 2a). As expected, the level of ablation of the GO surface is higher as the laser power increases. In Figures 2b-d we can appreciate how a higher laser power implies a higher thermal effect, thus leading to a wider effective path of the laser beam (increasement of around a 40% from 50 mW to 100 mW), as well as to a higher decrease of the LrGO thickness and a higher level of reduction (as demonstrated by the remaining non-reduced GO areas). The SEM images of Figure 2 also reveal the edges among the different layers which compose the GO structure [35], [47].

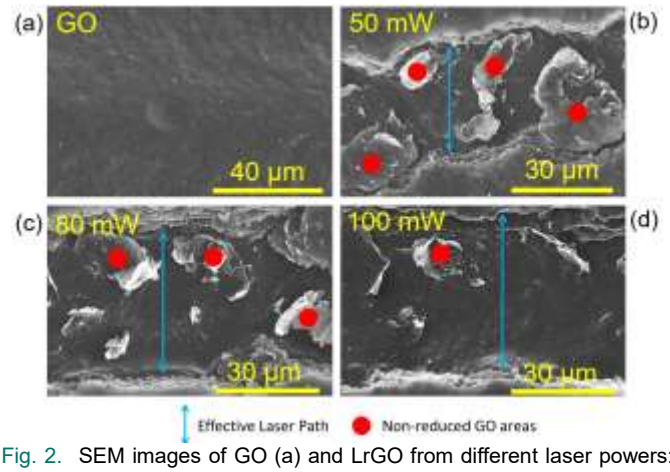

Fig. 2. SEM images of GO (a) and LrGO from different laser powers: 50 mW (b), 80 mW (c) and 100 mW (d).

The successful conversion from GO to LrGO is confirmed by the Raman spectroscopy results shown in Figure 3. This conversion is manifested by the increase of the ratio between the intensities of the G and D peaks, located at 1573 cm^{-1} and 1343 cm^{-1}, respectively. The G peak is intrinsically originated by the relative movement of the sp^2 hybridization bonds (graphitic signature of carbon), while the D is associated with the disorders induced by the defects on the sp^2 hybridized structure [48]. Additionally, the 2D peak (2678 cm^{-1}) is the result of a second order resonant process: the larger the ratio between the 2D and G peaks, the better the quality of the reduced graphene oxide [49]. As shown in Fig. 3a, the 2D peak is almost non-existent before the laser ablation of the GO surface. However, once the photothermal reduction is applied, the 2D peak emerges because of the healing of the crystallographic structure. As seen, the I_D/I_G ratio decreases at the same time that the I_{2D}/I_G ratio increases for higher laser reduction powers, which indicate that the rGO presents a less defective and disordered structure with respect to the GO precursor [43]. The improved structural ordering and the lower concentration of defects in the sp^2-hybridized carbon lattice of the LrGO as the laser power increases is also manifested through the narrowing of the full width at half-maximum (FWHM) of the 2D peak [50].

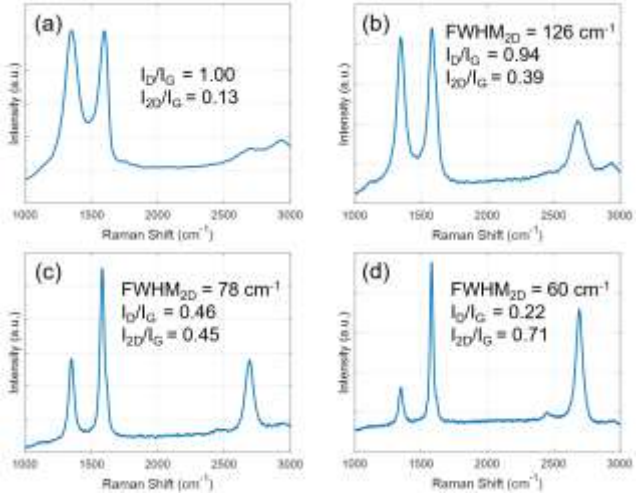

Fig. 3. Raman spectra of as-deposited GO before (a), and after the laser photothermal reduction for a laser power of 50 mW (b), 80 mW (c) and 100 mW (d).

The progressive reduction of the GO as the laser power increases can be analyzed by means of the XPS results at the different laser powers, as depicted in Figure 4. As seen, the UV laser treatment is able to reduce a large part of the oxygen-containing functional groups which compose the structure of the bare GO deposited on the flexible substrate. The analysis of the atomic concentrations extracted from the XPS results demonstrate an increase of the C/O ratio of up to a ~35% (see Table I). This increase is given mainly by the removal of the C-O bonds from the initial GO structure, as shown in Figures 4a-d. In addition to this, the relative increase of the C=C bonds after the laser photothermal process together with the emergence of the π-π* transition, which is a characteristic feature of sp^2 hybridization, indicate the healing of the crystallographic structure and supports the conversion from GO to rGO [51]–[53].

TABLE I. COMPARISON OF THE C/O RATIO BEFORE AND AFTER THE PHOTOTHERMAL PROCESS FOR THE DIFFERENT LASER POWERS.

Material	C/O Ratio
GO	2.236
LrGO@50mW	2.903
LrGO@80mW	3.023
LrGO@100mW	3.031

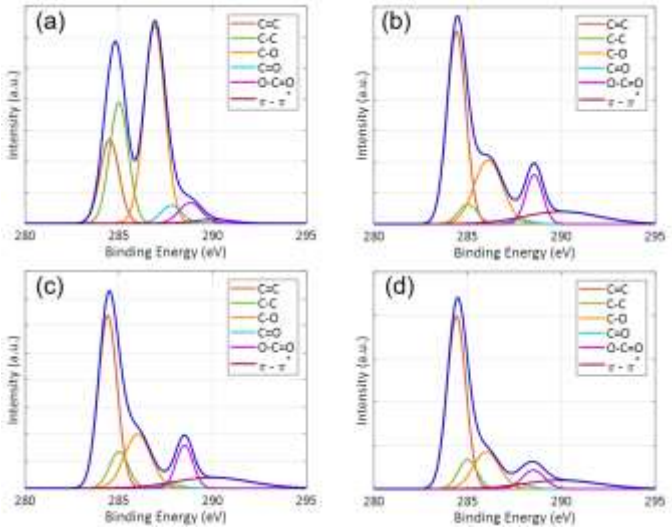

Fig. 4. High resolution C1s XPS spectra of the GO before (a), and after the laser photothermal reduction for the different laser powers: 50 mW (b), 80 mW (c) and 100 mW (d).

The gradual conversion from GO into rGO also comes with an increase of the conductivity of the resulting material as reported by the measurements of sheet resistance at the different laser powers. The results demonstrated that, although the typical sheet resistance of the bare GO is over 1 MΩ/sq., it can be significantly decreased down to around 500 Ω/sq. for a laser power of 50 mW, 280 Ω/sq. for 80 mW and 228 Ω/sq. for 100 mW, respectively. In addition, the impedance analyzer measurements for the devices at ambient conditions demonstrates that they present a pure resistive behavior at sub-GHz frequencies (see Figure 5).

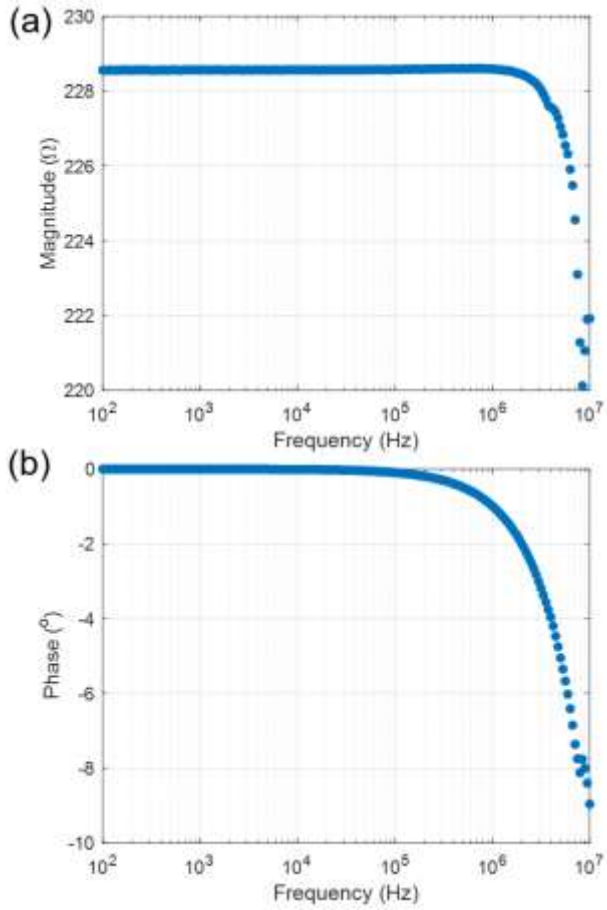

Fig. 5. Frequency response of an rGO@100mW sensor at ambient conditions. (a) Magnitude, (b) Phase.

B. Response to ammonia and ethanol

The resistance of the rGO-based sensors fabricated with different levels of reduction were tested at different concentrations of both ammonia and ethanol gases. The overall sensos' resistance can be expressed as the series combination of the resistance of the electrodes (R_e) and the resistance of the sensing layer (R_s) [44]. Considering that the resistance of the sensing layer is the only one affected by the gas exposure, the total resistance for a given concentration (c_1) can be written as:

$$R(c_1) = R_e + R_s(c_1) = R_e + R_s(c_0) + \Delta R_s(c_1) \quad (2)$$

being $R_s(c_0)$ the resistance of the sensing layer when it is not exposed to any testing gas.

Therefore, the normalized resistance variation can be reduced to Eq. 3, which manifests the relevance of increasing the dependency of the sensing layer resistance with respect to the gas concentration as well as decreasing the resistance of the electrode-sensing layer interface.

$$N.R. = \frac{R_e + R_s(c_1)}{R_e + R_s(c_0)} = 1 + \frac{\Delta R_s(c_1)}{R_e + R_s(c_0)} \quad (3)$$

Moreover, the hysteresis is calculated from Eq. 4, as the maximum difference of resistance obtained when increasing/decreasing the gas concentration with respect to the full scale [54]:

$$H(\%) = \frac{\max\left(\left|R(c_i)_{increasing} - R(c_i)_{decreasing}\right|\right)}{\max\left(R(c_i)\right) - \min\left(R(c_i)\right)} \cdot 100 \quad (4)$$

On this basis, Figure 6a details the response of the different devices towards ammonia at different concentrations using N_2 as carrier gas. The main features extracted from these results are summarized in Table II. Similarly, the response of the devices and their main features when they are exposed to the different ethanol concentrations are included in Figure 6b and Table III, respectively.

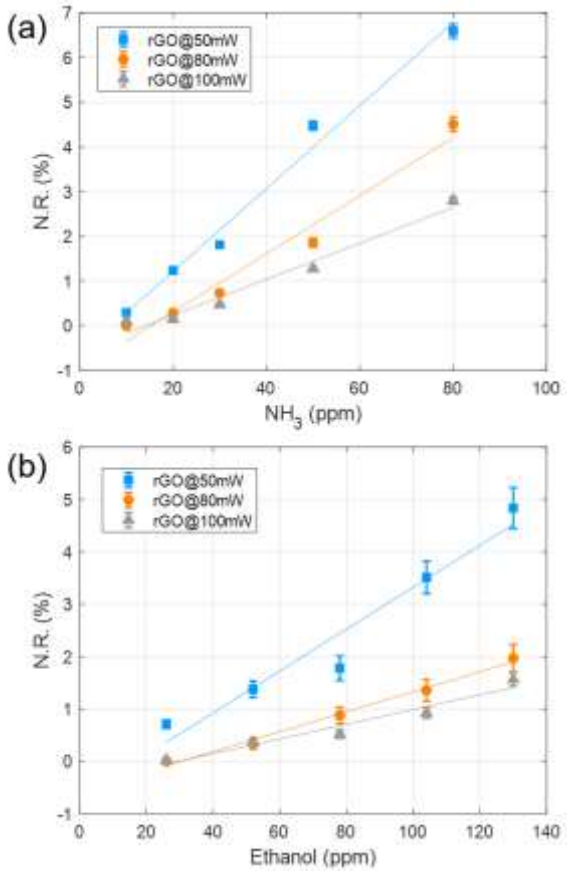

Fig. 6. Normalized Resistance as a function of different NH_3 (a) and ethanol (b) concentrations for rGO sensors with different level of reduction (Relative humidity: 55%).

TABLE II. COMPARISON OF THE MAIN FEATURES FOR AMMONIA SENSING.

Parameter	100 mW	80 mW	50 mW
Sensitivity (%/ppm)	0.0402 ± 0.001	0.0652 ± 0.002	0.0928 ± 0.002
Linearity (R^2)	0.9692	0.9688	0.9861
Hysteresis (%)	0.002	0.005	0.004

TABLE III. COMPARISON OF THE MAIN FEATURES AMONG FOR ETHANOL SENSING.

Parameter	100 mW	80 mW	50 mW
Sensitivity (%/ppm)	0.0140 ± 0.001	0.0191 ± 0.002	0.0390 ± 0.003
Linearity (R^2)	0.9474	0.9820	0.9425
Hysteresis (%)	0.002	0.004	0.005

The sensitivity was calculated by linear regression of the calibration curves presented in Figure 6. The dispersion was defined as the standard deviation of the sensitivities of different characterized devices. To study the stability and reproducibility of the sensors, we measured each sample 5 times.

IV. DISCUSSION

Although the sensors fabricated with the same laser power presented a slightly different overall resistance from one to another, the variation of their normalized resistance as a function of the testing gases is quite similar, as demonstrated by the standard deviation of the sensitivity for all cases. The increase of the resistance is given by the p-type property of rGO together with the electron acceptor of the gas molecules. The p-type semiconducting behaviour of GO depends on its degree of oxidation and therefore on the oxygen remaining on the carbon plane [55]. This, together with the higher presence of corrugations, breakages, and wrinkles to absorb the gas molecules, makes the less-reduced GO (rGO@50mW) more sensitive to the gas adsorption than the flat rGO films, as demonstrated for both ammonia and ethanol [56], [57]. The absorption of the gas molecules leads to a decrease of the LrGO conductivity, thus increasing the sensor resistance as the gas concentration increases. In general, the change in the sensors' resistance presents a relatively high linearity with respect to the gas concentration. However, it can also be seen that the more sensitive sensors are also more responsive as the target gas concentration increases due to both the higher absorption ability and the increase in the probability of adsorption of the gas molecules. This effect is handled in some works by defining two linear working regions (for lower and higher concentrations), as reported by Karaduman *et al.* [58] and Wang *et al.* [59] for their rGO-based gas sensors decorated with metal nanoparticles and ZnO/SnO_2, respectively. The lower sensitivity of LrGO for ethanol when compared with ammonia at room temperature was also reported in the literature for other resistive sensors based on GO [60]. This is a consequence of a better adsorption of the NH_3 molecules into the functional groups of the rGO layer when compared with the C_2H_5OH, likely attributable to its smaller molecule size. Moreover, the sensors present low hysteresis, for both gases, demonstrating that the high surface area of rGO is able to absorb the tested concentrations with no saturation and that the recovery procedure accomplishes the total desorption of the target gas molecules.

Table IV sums up the characteristics of the sensors develop and establish a comparison with respect to other rGO-based sensors reported in the literature. In our work, we selected as tested gases ammonia (NH_3) in a concentration range between

10 ppm and 100 ppm and ethanol (C_2H_5OH) covering the concentration range from 25 ppm to 130 ppm, in a similar way than Sha *et al*. [37], Chang *et al*. [61] and Feng *et al.* [62]. It is important to highlight that this work only considers the use raw LrGO as sensitive layer. Thus it simplifies the fabrication process when compared with other rGO-based sensors which, in addition to require the chemical reduction of GO, are also associated with the synthesis of other materials, such as Zinc Oxide (ZnO) composites [37], SnO_2 nanocrystals [61] or cobalt oxide (Co_3O_4) [62]. Moreover, the devices proposed in this work can operate at room temperature for both tested gases that, together with their purely resistive behavior, makes easier their integration in a final end-user device. Finally, although in this work we have considered the raw LrGO as sensitive layer, this technology can also be combined in future works with other materials to enhance their sensing properties.

TABLE IV. COMPARISON BETWEEN DIFFERENT RGO-BASED GAS SENSORS IN LITERATURE.

Ref.	Material	Tested Gases	Type	Sensitivity	Gas conc. Range (ppm)	Temp (ºC)
This work	rGO	Ethanol	Resistive	0.0140%/ppm (100 mW) 0.0191%/ppm (80 mW) 0.0390%/ppm (50 mW)	25 – 130	20- 25
Li et al. [20]	8ZTO/rGO		Resistive	0.973%/ppm (up to 100 ppm)	5 – 1200	275
Sha et al. [37]	rGO/ZnO		Amperometric	508.91 $\mu AmM^{-1}cm^{-2}$	23 – 230	400
Tang et al. [42]	MoO_3-rGO		Resistive	0.981%/ppm (up to 100 ppm)	10 – 8000	310
Chang et al. [61]	rGO/SnO_2		Resistive	56.818 %/ppm (up to 1.68 ppm)	0.56 – 1.68	300
This work	rGO	NH_3	Resistive	0.0402%/ppm (100 mW) 0.0652%/ppm (80 mW) 0.0928%/ppm (50 mW)	10 – 100	20 – 25
Feng et al. [62]	rGO/Co_3O_4 nanofiber		Resistive	1.072%/ppm (up to 50 ppm)	5 – 100	20
Huang et al. [36]	Chemically rGO		Resistive	0.742%/ppm (up to 50 ppm)	20 – 50	35

V. CONCLUSIONS

In this paper, we present ammonia and ethanol gas sensors based on laser reduced-graphene oxide reduced (LrGO) as sensitive layer. First, we analyzed the impedance response of the devices under no test exposure and observed that the devices present a low pass filter characteristic, with a phase of virtually zero up to 100 kHz, which yields a purely resistive characteristic. The results presented validate that the sensors based on LrGO are promising candidates for the detection of NH_3 and VOCs, like ethanol. In particular, LrGO exhibits higher sensitivity towards ammonia with a value of 0.0402%/ppm than ethanol (0.0140%/ppm) for a same level of GO reduction. In general, we observed that lower levels of GO reduction make the sensors more sensitive to gases absorption as a consequence of a higher p-type behavior and a higher presence of corrugations, breakages, and wrinkles to trap these molecules. We conclude that laser-reduced GO can rise a great attention for environmental monitoring of toxic gases, since it is proven as a cost-effective and a low energy process, thus contributing to the circular economy through the development of sustainable electronics.

ACKNOWLEDGMENTS

Authors want to thank Dr. Aniello Falco for the fruitful discussions that helped to improve the conducted research.

REFERENCES

[1] "Permissible Exposure Limits - Annotated Tables | Occupational Safety and Health Administration." https://www.osha.gov/annotated-pels (accessed Oct. 11, 2022).

[2] "EUR-Lex - 02000L0039-20100108 - EN - EUR-Lex." https://eur-lex.europa.eu/eli/dir/2000/39/2010-01-08 (accessed Oct. 11, 2022).

[3] M. Jagannathan, D. Dhinasekaran, A. R. Rajendran, and B. Subramaniam, "Selective room temperature ammonia gas sensor using nanostructured ZnO/CuO@graphene on paper substrate," *Sensors and Actuators B: Chemical*, vol. 350, p. 130833, Jan. 2022, doi: 10.1016/j.snb.2021.130833.

[4] Z. Zhang, D. Vedenov, and M. Wetzstein, "Can the US ethanol compete in the alternative fuels market?," *Agricultural Economics*, vol. 37, pp. 105–112, Jul. 2007, doi: 10.1111/j.1574-0862.2007.00228.x.

[5] A. S. Adekunle *et al.*, "Ethanol Sensor Based On Platinum-MWCNT-NiO Nanoparticles Platform Electrode," *Int. J. Electrochem. Sci.*, vol. 7, p. 15, 2012.

[6] F. A. Harraz, A. A. Ismail, A. A. Ibrahim, S. A. Al-Sayari, and M. S. Al-Assiri, "Highly sensitive ethanol chemical sensor based on nanostructured SnO2 doped ZnO modified glassy carbon electrode," *Chemical Physics Letters*, vol. 639, pp. 238–242, Oct. 2015, doi: 10.1016/j.cplett.2015.09.033.

[7] S. Liang *et al.*, "Deposition of cocoon-like ZnO on graphene sheets for improving gas-sensing properties to ethanol," *Applied Surface Science*, vol. 357, pp. 1593–1600, Dec. 2015, doi: 10.1016/j.apsusc.2015.10.033.

[8] J. Wang, Q. Zhou, S. Peng, L. Xu, and W. Zeng, "Volatile Organic Compounds Gas Sensors Based on Molybdenum Oxides: A Mini Review," *Front Chem*, vol. 8, p. 339, 2020, doi: 10.3389/fchem.2020.00339.

[9] Q. Zhou *et al.*, "Fabrication and characterization of highly sensitive and selective sensors based on porous NiO nanodisks," *Sensors and Actuators B: Chemical*, vol. 259, pp. 604–615, Apr. 2018, doi: 10.1016/j.snb.2017.12.050.

[10] J. Wang, Q. Zhou, Z. Lu, Z. Wei, and W. Zeng, "Gas sensing performances and mechanism at atomic level of Au-MoS2 microspheres," *Applied Surface Science*, vol. 490, pp. 124–136, Oct. 2019, doi: 10.1016/j.apsusc.2019.06.075.

[11] Z. Wei, Q. Zhou, and W. Zeng, "Hierarchical WO3-NiO microflower for high sensitivity detection of SF6 decomposition byproduct H2S," *Nanotechnology*, vol. 31, no. 21, Art. no. 21, May 2020, doi: 10.1088/1361-6528/ab73bd.

[12] M. He, Y. Wang, S. Wang, and S. Luo, "Laser-induced graphene enabled 1D fiber electronics," *Carbon*, vol. 168, pp. 308–318, Oct. 2020, doi: 10.1016/j.carbon.2020.06.084.

[13] A. Z. Yazdi, I. O. Navas, A. Abouelmagd, and U. Sundararaj, "Direct Creation of Highly Conductive Laser-Induced Graphene Nanocomposites from Polymer Blends," *Macromolecular Rapid Communications*, vol. 38, no. 17, p. 1700176, 2017, doi: 10.1002/marc.201700176.

[14] S. Srikanth, U. S. Jayapiriya, S. K. Dubey, A. Javed, and S. Goel, "Fabrication of ultra-thin laser induced graphene electrodes over negative photoresist on glass for various electronic applications," *Microelectronic Engineering*, vol. 259, p. 111790, Apr. 2022, doi: 10.1016/j.mee.2022.111790.

[15] Y. Houeix *et al.*, "Laser-synthesis of conductive carbon-based materials from two flexible commercial substrates: A comparison," *Applied Surface Science*, vol. 634, p. 157629, Oct. 2023, doi: 10.1016/j.apsusc.2023.157629.

[16] S. Kaur, D. Mager, J. G. Korvink, and M. Islam, "Unraveling the dependency on multiple passes in laser-induced graphene electrodes for supercapacitor and H2O2 sensing," *Materials Science for Energy Technologies*, vol. 4, pp. 407–412, Jan. 2021, doi: 10.1016/j.mset.2021.09.004.

[17] W. Ma, J. Zhu, Z. Wang, W. Song, and G. Cao, "Recent advances in preparation and application of laser-induced graphene in energy storage devices," *Materials Today Energy*, vol. 18, p. 100569, Dec. 2020, doi: 10.1016/j.mtener.2020.100569.

[18] A. A. Balandin, "Thermal properties of graphene and nanostructured carbon materials," *Nature Mater*, vol. 10, no. 8, Art. no. 8, Aug. 2011, doi: 10.1038/nmat3064.

[19] S. Evlashin *et al.*, "Controllable Laser Reduction of Graphene Oxide Films for Photoelectronic Applications," *ACS Appl. Mater. Interfaces*, vol. 8, no. 42, pp. 28880–28887, Oct. 2016, doi: 10.1021/acsami.6b10145.

[20] Y. Li *et al.*, "In situ decoration of Zn2SnO4 nanoparticles on reduced graphene oxide for high performance ethanol sensor," *Ceramics International*, vol. 44, no. 6, pp. 6836–6842, Apr. 2018, doi: 10.1016/j.ceramint.2018.01.107.

[21] B. G. Ghule *et al.*, "Natural Carbonized Sugar as a Low-Temperature Ammonia Sensor Material: Experimental, Theoretical, and Computational Studies," *ACS Appl. Mater. Interfaces*, vol. 9, no. 49, pp. 43051–43060, Dec. 2017, doi: 10.1021/acsami.7b13122.

[22] L. A. Panes-Ruiz *et al.*, "Toward Highly Sensitive and Energy Efficient Ammonia Gas Detection with Modified Single-Walled Carbon Nanotubes at Room Temperature," *ACS Sens.*, vol. 3, no. 1, pp. 79–86, Jan. 2018, doi: 10.1021/acssensors.7b00358.

[23] X. Liu *et al.*, "Enhanced X-ray photon response in solution-synthesized CsPbBr3 nanoparticles wrapped by reduced graphene oxide," *Solar Energy Materials and Solar Cells*, vol. 187, pp. 249–254, Dec. 2018, doi: 10.1016/j.solmat.2018.08.009.

[24] A. H. Chowdhury, N. Salam, R. Debnath, Sk. M. Islam, and T. Saha, "Chapter 8 - Design and Fabrication of Porous Nanostructures and Their Applications," in *Nanomaterials Synthesis*, Y. Beeran Pottathara, S. Thomas, N. Kalarikkal, Y. Grohens, and V. Kokol, Eds., in Micro and Nano Technologies. Elsevier, 2019, pp. 265–294. doi: 10.1016/B978-0-12-815751-0.00008-0.

[25] J. Guo, R. Wen, J. Zhai, and Z. L. Wang, "Enhanced NO2 gas sensing of a single-layer MoS2 by photogating and piezo-phototronic effects," *Science Bulletin*, vol. 64, no. 2, pp. 128–135, Jan. 2019, doi: 10.1016/j.scib.2018.12.009.

[26] S.-Y. Cho *et al.*, "Highly Enhanced Gas Adsorption Properties in Vertically Aligned MoS2 Layers," *ACS Nano*, vol. 9, no. 9, pp. 9314–9321, Sep. 2015, doi: 10.1021/acsnano.5b04504.

[27] Abhay. V. Agrawal *et al.*, "Photoactivated Mixed In-Plane and Edge-Enriched p-Type MoS2 Flake-Based NO2 Sensor Working at Room Temperature," *ACS Sens.*, vol. 3, no. 5, pp. 998–1004, May 2018, doi: 10.1021/acssensors.8b00146.

[28] D. J. Late *et al.*, "Sensing Behavior of Atomically Thin-Layered MoS2 Transistors," *ACS Nano*, vol. 7, no. 6, pp. 4879–4891, Jun. 2013, doi: 10.1021/nn400026u.

[29] H. Li *et al.*, "Fabrication of single- and multilayer MoS2 film-based field-effect transistors for sensing NO at room temperature," *Small*, vol. 8, no. 1, pp. 63–67, Jan. 2012, doi: 10.1002/smll.201101016.

[30] A. Agrawal, N. Kumar, and M. Kumar, "Strategy and Future Prospects to Develop Room-Temperature-Recoverable NO2 Gas Sensor Based on Two-Dimensional Molybdenum Disulfide," *Nano-Micro Letters*, vol. 13, Jan. 2021, doi: 10.1007/s40820-020-00558-3.

[31] F. Schedin *et al.*, "Detection of individual gas molecules adsorbed on graphene," *Nature Mater*, vol. 6, no. 9, Art. no. 9, Sep. 2007, doi: 10.1038/nmat1967.

[32] B. Sriram, M. Govindasamy, S.-F. Wang, R. Jothi Ramalingam, H. Al-lohedan, and T. Maiyalagan, "Novel sonochemical synthesis of Fe3O4 nanospheres decorated on highly active reduced graphene oxide nanosheets for sensitive detection of uric acid in biological samples," *Ultrasonics Sonochemistry*, vol. 58, p. 104618, Nov. 2019, doi: 10.1016/j.ultsonch.2019.104618.

[33] M. Govindasamy, S.-F. Wang, S. Kumaravel, R. J. Ramalingam, and H. A. Al-Lohedan, "Facile synthesis of copper sulfide decorated reduced graphene oxide nanocomposite for high sensitive detection of toxic

antibiotic in milk," *Ultrason Sonochem*, vol. 52, pp. 382–390, Apr. 2019, doi: 10.1016/j.ultsonch.2018.12.015.

[34] R. Ghosh, A. Singh, S. Santra, S. K. Ray, A. Chandra, and P. K. Guha, "Highly sensitive large-area multi-layered graphene-based flexible ammonia sensor," *Sensors and Actuators B: Chemical*, vol. 205, pp. 67–73, Dec. 2014, doi: 10.1016/j.snb.2014.08.044.

[35] Z. Wan *et al.*, "Tuning the sub-processes in laser reduction of graphene oxide by adjusting the power and scanning speed of laser," *Carbon*, vol. 141, pp. 83–91, Jan. 2019, doi: 10.1016/j.carbon.2018.09.030.

[36] X. Huang, N. Hu, L. Zhang, L. Wei, H. Wei, and Y. Zhang, "The NH3 sensing properties of gas sensors based on aniline reduced graphene oxide," *Synthetic Metals*, vol. 185–186, pp. 25–30, Dec. 2013, doi: 10.1016/j.synthmet.2013.09.034.

[37] R. Sha, S. K. Puttapati, V. V. S. S. Srikanth, and S. Badhulika, "Ultra-Sensitive Non-Enzymatic Ethanol Sensor Based on Reduced Graphene Oxide-Zinc Oxide Composite Modified Electrode," *IEEE Sensors Journal*, vol. 18, no. 5, pp. 1844–1848, Mar. 2018, doi: 10.1109/JSEN.2017.2787538.

[38] Q. Feng, X. Li, J. Wang, and A. M. Gaskov, "Reduced graphene oxide (rGO) encapsulated Co3O4 composite nanofibers for highly selective ammonia sensors," *Sensors and Actuators B: Chemical*, vol. 222, pp. 864–870, Jan. 2016, doi: 10.1016/j.snb.2015.09.021.

[39] X. Huang *et al.*, "Reduced graphene oxide–polyaniline hybrid: Preparation, characterization and its applications for ammonia gas sensing," *J. Mater. Chem.*, vol. 22, no. 42, pp. 22488–22495, Oct. 2012, doi: 10.1039/C2JM34340A.

[40] M. Sangeetha and D. Madhan, "Ultra sensitive molybdenum disulfide (MoS2)/graphene based hybrid sensor for the detection of NO2 and formaldehyde gases by fiber optic clad modified method," *Optics & Laser Technology*, vol. 127, p. 106193, Jul. 2020, doi: 10.1016/j.optlastec.2020.106193.

[41] M. Tian, J. Miao, P. Cheng, H. Mu, J. Tu, and J. Sun, "Layer-by-layer nanocomposites consisting of Co3O4 and reduced graphene (rGO) nanosheets for high selectivity ethanol gas sensors," *Applied Surface Science*, vol. 479, pp. 601–607, Jun. 2019, doi: 10.1016/j.apsusc.2019.02.148.

[42] Z. Tang *et al.*, "MoO3 nanoflakes coupled reduced graphene oxide with enhanced ethanol sensing performance and mechanism," *Sensors and Actuators B: Chemical*, vol. 297, p. 126730, Oct. 2019, doi: 10.1016/j.snb.2019.126730.

[43] F. J. Romero *et al.*, "Design guidelines of laser reduced graphene oxide conformal thermistor for IoT applications," *Sensors and Actuators A: Physical*, vol. 274, pp. 148–154, May 2018, doi: 10.1016/j.sna.2018.03.014.

[44] F. J. Romero *et al.*, "In-Depth Study of Laser Diode Ablation of Kapton Polyimide for Flexible Conductive Substrates," *Nanomaterials*, vol. 8, no. 7, Art. no. 7, Jul. 2018, doi: 10.3390/nano8070517.

[45] A. Abdellah *et al.*, "Flexible Carbon Nanotube Based Gas Sensors Fabricated by Large-Scale Spray Deposition," *IEEE Sensors Journal*, vol. 13, no. 10, pp. 4014–4021, Oct. 2013, doi: 10.1109/JSEN.2013.2265775.

[46] F. Loghin, A. Abdellah, A. Falco, M. Becherer, P. Lugli, and A. Rivadeneyra, "Time stability of carbon nanotube gas sensors," *Measurement*, vol. 136, pp. 323–325, Mar. 2019, doi: 10.1016/j.measurement.2018.12.097.

[47] Y. C. Guan, Y. W. Fang, G. C. Lim, H. Y. Zheng, and M. H. Hong, "Fabrication of Laser-reduced Graphene Oxide in Liquid Nitrogen Environment," *Sci Rep*, vol. 6, no. 1, Art. no. 1, Jun. 2016, doi: 10.1038/srep28913.

[48] F. Tuinstra and J. L. Koenig, "Raman Spectrum of Graphite," *Journal of Chemical Physics*, vol. 53, pp. 1126–1130, Aug. 1970, doi: 10.1063/1.1674108.

[49] A. C. Ferrari *et al.*, "Raman Spectrum of Graphene and Graphene Layers," *Phys. Rev. Lett.*, vol. 97, no. 18, p. 187401, Oct. 2006, doi: 10.1103/PhysRevLett.97.187401.

[50] S. Grimm, M. Schweiger, S. Eigler, and J. Zaumseil, "High-Quality Reduced Graphene Oxide by CVD-Assisted Annealing," *J. Phys. Chem. C*, vol. 120, no. 5, pp. 3036–3041, Feb. 2016, doi: 10.1021/acs.jpcc.5b11598.

[51] H. Estrade-Szwarckopf, "XPS photoemission in carbonaceous materials: A 'defect' peak beside the graphitic asymmetric peak," *Carbon*, vol. 42, no. 8, pp. 1713–1721, Jan. 2004, doi: 10.1016/j.carbon.2004.03.005.

[52] Q. Yuan, C.-T. Lin, and K. W. A. Chee, "All-carbon devices based on sp^2 -on-sp^3 configuration," *APL Materials*, vol. 7, no. 3, p. 030901, Mar. 2019, doi: 10.1063/1.5082767.

[53] M. C. Biesinger, "Accessing the robustness of adventitious carbon for charge referencing (correction) purposes in XPS analysis: Insights from a multi-user facility data review," *Applied Surface Science*, vol. 597, p. 153681, Sep. 2022, doi: 10.1016/j.apsusc.2022.153681.

[54] S. Beeby, Ed., *MEMS mechanical sensors*. in Artech House microelectromechanical system series. Boston: Artech House, 2004.

[55] D.-T. Phan and G.-S. Chung, "P–n junction characteristics of graphene oxide and reduced graphene oxide on n-type Si(111)," *Journal of Physics and Chemistry of Solids*, vol. 74, no. 11, pp. 1509–1514, Nov. 2013, doi: 10.1016/j.jpcs.2013.02.007.

[56] S. Yol Jeong *et al.*, "Enhanced response and sensitivity of self-corrugated graphene sensors with anisotropic charge distribution," *Sci Rep*, vol. 5, no. 1, Art. no. 1, Jun. 2015, doi: 10.1038/srep11216.

[57] S. J. Young and Z. D. Lin, "Ammonia gas sensors with Au-decorated carbon nanotubes," *Microsyst Technol*, vol. 24, no. 10, pp. 4207–4210, Oct. 2018, doi: 10.1007/s00542-018-3712-x.

[58] I. Karaduman, E. Er, H. Çelikkan, N. Erk, and S. Acar, "Room-temperature ammonia gas sensor based on reduced graphene oxide nanocomposites decorated by

Ag, Au and Pt nanoparticles," *Journal of Alloys and Compounds*, vol. 722, pp. 569–578, Oct. 2017, doi: 10.1016/j.jallcom.2017.06.152.
[59] Z. Wang, S. Gao, T. Fei, S. Liu, and T. Zhang, "Construction of ZnO/SnO2 Heterostructure on Reduced Graphene Oxide for Enhanced Nitrogen Dioxide Sensitive Performances at Room Temperature," *ACS Sens.*, vol. 4, no. 8, pp. 2048–2057, Aug. 2019, doi: 10.1021/acssensors.9b00648.
[60] R. Kumar and R. Ghosh, "Selective determination of ammonia, ethanol and acetone by reduced graphene oxide based gas sensors at room temperature," *Sensing and Bio-Sensing Research*, vol. 28, p. 100336, Jun. 2020, doi: 10.1016/j.sbsr.2020.100336.
[61] Y. Chang, Y. Yao, B. Wang, H. Luo, T. Li, and L. Zhi, "Reduced Graphene Oxide Mediated SnO2 Nanocrystals for Enhanced Gas-sensing Properties," *Journal of Materials Science & Technology*, vol. 29, no. 2, pp. 157–160, Feb. 2013, doi: 10.1016/j.jmst.2012.11.007.
[62] Q. Feng, X. Li, J. Wang, and A. M. Gaskov, "Reduced graphene oxide (rGO) encapsulated Co3O4 composite nanofibers for highly selective ammonia sensors," *Sensors and Actuators B: Chemical*, vol. 222, pp. 864–870, Jan. 2016, doi: 10.1016/j.snb.2015.09.021.

ALMUDENA RIVADENEYRA obtained the master's degrees in telecommunication engineering, environmental sciences, and electronics engineering from the University of Granada, Spain, in 2009, 2009, and 2012, respectively, and the Ph.D. degree in design and development of environmental sensors from the University of Granada in 2014. She was with the Institute for Nanoelectronics, Technical University of Munich and currently is a Ramón y Cajal Fellow at the University of Granada. She obtained the Young Researcher Award in 2019 by the Consejo Social UGR and a Marie Curie Fellowship in 2018. Her work is centred in printed and flexible electronics with a special focus on sensors and RFID technology.

DENICE GERARDO received the engineering degree in Renewable Energies from the Technological University of Culiacan (UTC), Sinaloa, Mexico in 2017 and the master degree in Biological Sciences from the Autonomous University of Sinaloa (UAS), Mexico, in 2022. She had a national scholarship National Quality Postgraduate Program (PNPC) of CONACYT from 2020 to 2022 to participate in exchange programs with the University of Granada (Spain). She is currently working at the Dept. of Electronics and Computer technology of the University of Granada. Her current research interests include the laser nano structuring of organic materials for biomedical and electronics applications.

FRANCISCO J. ROMERO received the B.Eng. in Telecommunication Engineering from the University of Granada (Spain) in 2016, and the M.Eng. in Telecommunications Engineering from the University of Granada in 2018, both with valedictorian mention. In 2015, he joined the Department of Electronics and Computer Technology at the University of Granada as Ungraduated Researcher, and obtained a national predoctoral scholarship in 2017. He defended his Ph.D in Flexible Sensors for IoT Applications using Emerging Technologies in 2021. He is currently a Postdoc at the University of Granada. His current research interest includes graphene-based sensors, flexible electronics and IoT embedded systems.

VÍCTOR TORAL received the B.Eng. degree in electronic engineering from the University of Granada, in 2017, and the M.Eng. degree in electronics engineering from the Polytechnic University of Madrid, in 2018. He recently got the Ph.D. degree with the Department of Electronics and Computer Technology, University of Granada. His current research interests include biosignals acquisition devices, reconfigurable instrumentation, and flexible electronics.

SAHIRA VASQUEZ graduated as a Food Technology Engineer from ISA University, Dominican Republic (2013). She received her M.Sc. degree in Environmental Protection and Food Agricultural Production from Hohenheim University, Germany (2015). Since 2019, she is a Ph.D. student in the program Food Engineering and Biotechnology at the Free University of Bozen-Bolzano, Italy. Her research line is focused on the development of printed sensors to monitor byproducts (e.g., gases) of fermentative processes on in-vitro systems.

MARTINA COSTA-ANGELI obtained the master's degree in biomedical engineering (2016) from Politecnico di Milano (Italy), where she obtained the Ph.D. in materials engineering in 2020 working on the development of different types of deformable printed low-cost sensors for strain measurement. Currently, she is an assistant professor at the Sensing Technologies Lab of Free University of Bolzano (Italy). Her current research work is focusing on the design of low-cost flexible sensors for environmental and human monitoring, and food safety.

CARMEN L. MORAILA-MARTINEZ received the M.Sc. degrees in Physics from the University of San Luis Potosí, México and in Colloids and interfaces science and technology from the University of Granada, Spain in 2008 and 2010, respectively, and the Ph.D. degree in Physics and Space Sciences from the University of Granada, Spain, in 2012. She was an Associate Professor with the Physics and Mathematics department, University of Sinaloa, México and currently she is María Zambrano Fellow with the University of Granada, where her work is centred in printed and flexible electronics with a special focus on sensors for biological applications.

DIEGO P. MORALES obtained o the M.Sc. degree in electronic engineering and the Ph.D. degree in electronic engineering from the University of Granada, Granada, Spain, in 2001 and 2011, respectively. He was an Associate Professor with the Department of Computer Architecture and Electronics, University of Almería, Spain. After that, he joined the Department of Electronics and Computer Technology, University of Granada, where he currently serves as a Full Professor. His current research interest includes developing reconfigurable applications.

NOEL RODRIGUEZ received the B.Eng. with a first national award and M.Eng. in Electronics Engineering from the University of Granada, Spain, in 2004 and 2006 respectively. In 2008, he received a double Ph.D. from the University of Granada and the Institute National Polytechnique of Grenoble. He is currently Full Professor at the University of Granada. His research interest includes the development of new technologies for ubiquitous electronics, and the development of low-power energy adapters.